The effect of hydrogen on the electronic and bonding properties of amorphous carbon

2006 J. Phys.: Condens. Matter 18 10803

(http://iopscience.iop.org/0953-8984/18/48/007)

INSTITUTE OF PHYSICS PUBLISHING JOURNAL OF PHYSICS: CONDENSED MATTER

J. Phys.: Condens. Matter **18** (2006) 10803–10815 doi:10.1088/0953-8984/18/48/007

The effect of hydrogen on the electronic and bonding properties of amorphous carbon

J T Titantah[1], D Lamoen[1], E Neyts[2] and A Bogaerts[2]

[1] TSM, Departement Fysica, Universiteit Antwerpen, Groenenborgerlaan 171, 2020 Antwerpen, Belgium
[2] PLASMANT, Departement Chemie, Universiteit Antwerpen, Universiteitsplein 1, 2610 Antwerpen, Belgium

Received 18 July 2006, in final form 5 October 2006
Published 17 November 2006
Online at stacks.iop.org/JPhysCM/18/10803

Abstract

A series of amorphous carbon and hydrogen-containing amorphous carbon structures has been generated, by using classical Monte Carlo and molecular dynamics simulation techniques, respectively. The Brenner empirical bond order potential is used to generate hydrogenated amorphous carbon while that by Tersoff is used for amorphous carbon. The resulting structures are relaxed further using the density functional theory approach. Structures containing 15 at.% hydrogen are generated for various mass densities in order to investigate the effect of pressure changes on the properties of the hydrogenated amorphous carbon. The structures are analysed in terms of their sp^3/sp^2 ratio. The density of states (DOS), energy-loss near-edge structure (ELNES) and x-ray photoelectron spectroscopy (XPS) calculations are performed within the first-principles methodology on the generated carbon systems. The ELNES and the C 1s energy calculations are performed taking into account the core–hole effect. Our calculations show that depending on the density ρ, hydrogenated amorphous carbon can be classified into three categories: polymeric at low densities ($\rho \leqslant 2.0$ g cm^{-3}), graphitic at intermediate densities (2.0 g cm^{-3} $< \rho \leqslant 2.4$ g cm^{-3}) and diamond-like at high densities ($\rho > 2.4$ g cm^{-3}).

1. Introduction

Most amorphous carbon (a-C) structures contain hydrogen contaminants inherent of the precursors involved in their synthesis. On the other hand, hydrogen can be intentionally inserted into a-C in order to tailor its electronic, optical, tribological and mechanical properties for special applications. For example, hydrogen is important for obtaining a wide band gap and high electrical resistivity [1]. Hydrogen stabilizes the diamond-like structure by maintaining the sp^3 carbon content, thereby enabling its usage for coating of cutting tools, high shear stress devices, solar cells and hard discs. Amorphous carbon with a high sp^3 carbon content is generally referred to as diamond-like carbon (DLC). A review of DLC films is found in [2].

The theoretical work on the effect of hydrogen on the electronic properties of a-C is still very limited, despite tremendous experimental efforts devoted to the synthesis and characterization of hydrogenated amorphous carbon (a-C:H) [2–10]. Most of the available theoretical work is devoted to the deposition and structural characterization [11–17] and, to a lesser extent, to the calculation of the electronic density of states (DOS) [18–21]. There is practically no theoretical work available on the energy-loss near-edge structure (ELNES) or the x-ray absorption near-edge structure (XANES) of a-C:H. XANES spectra exist [3, 6] for a-C:H systems, and their interpretation is often done by comparison with the spectra of crystalline graphite and diamond and those of some organic polymers [22, 23]. Also, x-ray photoelectron spectroscopy (XPS) is widely used to characterize DLC films [4, 8, 24, 25], but again with no theoretical counterpart. C 1s core-level shifts have been calculated for amorphous carbon [26], amorphous carbon nitrides [27] and some organic polymers [28].

One of the early theoretical studies on a-C:H is that by Frauenheim *et al* [18]. In this work a semi-empirical molecular dynamics approach was adopted for the generation of the a-C:H systems. The bonding structure was characterized by calculating the fraction of four-coordinated carbon atoms in these structures. Their calculations showed that as the density was increased from 2.0 to 2.2 g cm^{-3} the fraction of four-coordinated atoms increased but on further increase to 2.4 g cm^{-3} there was no major change in this fraction. Above 2.4 g cm^{-3} it was shown to grow monotonically with increasing density. This was the case for a-C:H with a hydrogen content of $\geqslant$20%. At a hydrogen content of 20 at.% and at a density of 2.7 g cm^{-3} the fraction of four-coordinated carbon atoms was about 35%. This value is very low even when compared with the sp^3 fraction of hydrogen-free a-C measured using the ELNES techniques at such densities, since it is an established fact that hydrogen increases this fraction in a-C:H [29]. In computer-generated carbon systems the fraction of four-coordinated atoms is usually assimilated with that of the sp^3-hybridized carbon atoms in these structures. However, it was recently shown that curvature effects on three-coordinated atoms can lead to a higher sp^3 fraction [26]. Within a density functional theory (DFT) approach, Iarlori *et al* [11] obtained 41% four-fold and 56% three-fold carbon atoms for a 16 at.% H a-C:H system at a density of 2.6 g cm^{-3}.

The Brenner bond order empirical potential [30] is widely used in the study of the DLC deposition process [13, 14, 16, 17]. This potential is known to underestimate the amount of four-coordinated carbon atoms in a-C:H. A recent study of the quantum effects on the erosion of carbon-based materials as a result of a bombardment with hyperthermal ions revealed that the Brenner potential with a cut-off distance of 2.0 Å is not appropriate [15]. When the cut-off was increased to 2.46 Å, results obtained using the tight-binding molecular dynamics calculations were reproduced. A similar conclusion was obtained by us [31] for the Tersoff potential [32]—another bond-order type of potential.

In this work, we generate amorphous carbon and hydrogenated amorphous carbon samples using the Tersoff and the Brenner bond order empirical potentials, respectively. The resulting structures are relaxed further using a DFT approach [33] within the local density approximation [34]. We show that DFT relaxation strongly modifies the a-C:H structures generated using the Brenner potential. We study the electronic properties of the generated a-C:H systems by calculating the DOS, ELNES and XPS spectra. Comparison is made with calculations on hydrogen-free amorphous carbon, and the effect of hydrogen is pointed out. The rest of the paper is organized as follows. In section 2 a brief description of the computational methods used is given. In section 3 the structure of the generated systems is analysed by looking at the pair correlation functions, the bond angle distribution and the end-to-end distance distribution of chains of four trigonal atoms. This distribution can be used as a probe of possible sp^2 bond clustering. The DOS and the C 1s spectroscopies

(ELNES and XPS) are presented in section 4. A summary of the main results is presented in section 5.

2. Computational details

We generated amorphous carbon structures by means of classical Monte Carlo (MC) simulations based on Tersoff's empirical potential for carbon [32]. The potential was developed in line with the empirical chemical pseudopotential theory of Abell [35] in which the bonding environment is mimicked through a bond order term. We adjusted the cut-off distance of this potential to 2.4 Å in order to correctly locate the second neighbour atomic shell and to yield the correct relationship between the sp^3 bonding fraction and the carbon density. The original cut-off of 2.1 Å yields an sp^3 fraction of ∼40% at a density of 3.4 g cm^{-3}, but adjusting this cut-off to 2.4 Å yields an sp^3 fraction $\geqslant$80%, which is expected for such high-density amorphous carbon [29]. By quenching hot liquid carbon from 5000 K down to 300 K we generated amorphous carbon structures at densities ranging from 1.75 to 3.5 g cm^{-3} via a continuous space, periodic boundary condition (PBC), constant volume, constant temperature and constant number of atoms classical Metropolis MC procedure on cubic cells made of 64 atoms.

Using classical molecular dynamics simulations, a set of a-C:H structures was created at densities ranging from 1.5 to 3.0 g cm^{-3}. The interatomic potential used is the Brenner potential for hydrocarbons, which is basically a modified version of the Tersoff potential. The Brenner potential includes additional functions for describing the different chemistry of C and H, and allows a better description of intermediate bonding situations, such as the overbinding of radicals and conjugation effects [30]. The upper cut-off limits for C–C, C–H and H–H interactions are 2.0, 1.8 and 1.7 Å, respectively. The structures were created by simulated deposition at 100 K, in which consecutive low-energy hydrocarbon radicals allowed for film growth. During these simulations, periodic boundaries were applied in the lateral directions. The bottom atomic layers were held rigid to anchor the simulation cell. During each hydrocarbon impact, the simulation was carried out under constant volume, constant number of atoms and constant energy conditions, corresponding to the microcanonical ensemble. After each impact, a Berendsen heat bath was applied to thermalize the growing film back to 100 K. After the final film was obtained, the film was allowed to relax for 10 ps. The resulting films consisted of 82 carbon atoms and 15 hydrogen atoms, resulting in 15.5 at.% H.

The resulting a-C:H structures were further relaxed using the DFT approach. Only the a-C structures at densities of 2.0, 2.4 and 2.8 g cm^{-3} were relaxed further with DFT. For the DFT relaxation, the forces on the nuclei are used to displace the atoms using a damped Newton dynamics [36]. The position of each atom at the next step is determined from that of the previous and the present steps and the force as

$$R_m^{\tau+1} = R_m^{\tau} + \eta_m(R_m^{\tau} - R_m^{\tau-1}) + \delta_m F_m^{\tau}, \tag{1}$$

where R_m^{τ} and F_m^{τ} are the coordinate and respective force at step τ; meanwhile η_m and δ_m control the damping and the speed of the motion of the particles. These parameters are chosen such that the particles move more quickly towards the closest local minimum and with little or no oscillation around this minimum. Atoms were moved until the magnitude of the force on each atom was less than 10 mRyd/bohr.

The DFT calculations were performed using the all-electron full-potential-(linearized)-augmented-plane-wave + local orbital code WIEN2k [33]. The exchange and correlation potential was treated using the local density approximation [34]. Muffin-tin radii (R_{MT}) were fixed at 0.65 atomic units (au) and 1.0 au for the hydrogen and carbon atoms, respectively. The plane wave cut-off parameter $R_{\mathrm{MT}} \times K_{\max}$ ($K_{\max}$ being the plane wave cut-off) values of

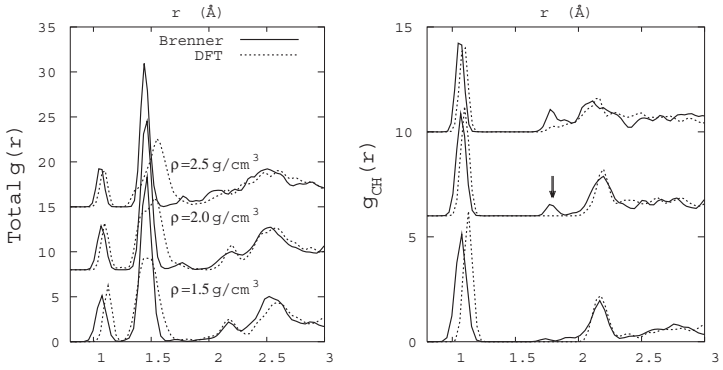

Figure 1. Total (left) and C–H (right) pair correlation functions for hydrogen-containing amorphous carbon at mass densities of 1.5, 2.0 and 2.5 g cm^{-3}. Structures generated using the Brenner potential show a C–H feature separated by a distance of 1.8 Å (see arrow in the right panel). After DFT relaxation this feature vanishes.

5.0 for the a-C and 3.0 for the a-C:H systems were adopted for the calculations. 100 k-points were used to sample the full Brillouin zone of the systems, i.e. 32 points in the corresponding irreducible Brillouin zones. The C 1s energies were evaluated within the DFT methodology as described in [26]. One electron was removed from the 1s state and inserted as a uniform background charge in the DFT calculation (the core-excited state). A ground state calculation was performed, and the Fermi energy corrected total energy difference between the core-excited and the ground state gave the core-level energy. This approach localized the C 1s energy of graphite at 284.6 eV and that of diamond at 285.5 eV, which is in excellent agreement with experiment [37]. In order to get the core-level energy distribution for each amorphous carbon system, self-consistent core–hole calculations were repeated for all atoms of the generated structures, i.e. 64 calculations for each of the a-C systems and 82 for each a-C:H system. The C 1s ELNES spectra were also calculated within the core-excited approach.

The coordination structure of each carbon atom in the generated systems was obtained by counting the number of atoms within a sphere of radius 1.9 Å (first minimum in the C–C pair correlation function) centred on each atom.

3. Structural analysis

In order to study the effect of using the Brenner potential with C–H and C–C cut-off distances of 1.8 Å and 2.0 Å, respectively, we show in figure 1 the total and C–H pair correlation functions of the a-C:H structures generated using the Brenner potential and the same functions after DFT relaxation. Notice that when the Brenner potential is used the C–H pair correlation function shows features at 1.09 Å (the equilibrium C–H bond length), 1.8 Å and 2.15 Å. After DFT relaxation the feature at 1.8 Å vanishes. This feature might have resulted from the choice of the range of the C–H potential. Using a tight-binding (TB) model Godwin *et al* [12] noticed the presence of this C–H feature in their C–H pair correlation function. They suggested that this feature could be an artefact of the short cut-off distance of 1.85 Å used for the C–H TB potential. A DFT-based calculation [11] did not show such a feature. Another effect of the DFT relaxation is the change in the C–C first-neighbour shell. It becomes broader and shifts to higher distances in agreement with the transition from the graphitic bond length (1.42 Å) to the diamond bond length (1.54 Å). A more serious issue is the underestimation of the sp^3 carbon

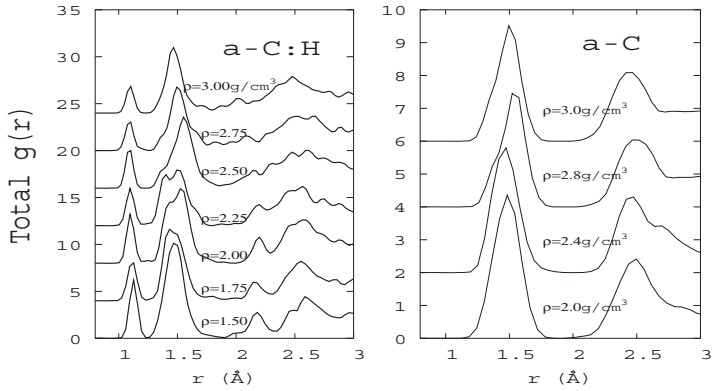

Figure 2. Total pair correlation functions for hydrogen-containing amorphous carbon (left) and hydrogen-free amorphous carbon (right) at various mass densities. All structures have been relaxed using the DFT approach.

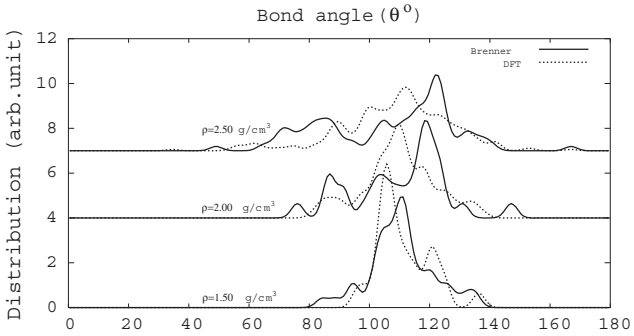

Figure 3. Bond angle distribution for structures generated using the Brenner potential and their subsequent relaxation with DFT. After DFT relaxation the bond angle distribution becomes broader and shifts to the tetrahedral bond angles for intermediate and higher densities.

fraction in systems generated using the short-range Brenner potential [38]. This problem is also encountered when the Tersoff potential is used to generate a-C structures. Recently we showed that on increasing the range of the Tersoff potential to 2.4 Å a drastic improvement in the relation between the density and the sp^3 fraction was obtained [26]. However, the Brenner potential reproduces the C–H bond length and the C–C second-neighbour shell very well.

For comparison, the radial distribution functions of the hydrogen-free and hydrogen-containing amorphous carbon systems are shown in figure 2. Note that the insertion of hydrogen gives a radial distribution function with many features, especially in the second-neighbour shell, indicating that hydrogen leads to a more disordered carbon structure. The radial distribution functions show that at intermediate densities ($2.0\ \mathrm{g\ cm^{-3}} < \rho \leqslant 2.4\ \mathrm{g\ cm^{-3}}$) C=C double bonds with bond lengths of 1.35 ± 0.01 Å are seen to be present in the a-C:H systems. Careful analysis of our generated structures reveals that the same 1.35 Å feature is still present at lower densities, though not visible in the $g(r)$ because of its overlap with 1.4 Å feature. At a density of $2.0\ \mathrm{g\ cm^{-3}}$ Jungnickel *et al* [19] reported such bonds in a 33 at.% H a-C:H system generated using a semi-empirical density-functional molecular dynamics simulation.

Another structural property of interest is the distribution of bond angles (see figure 3). This distribution is plotted for structures generated using the Brenner potential and those obtained

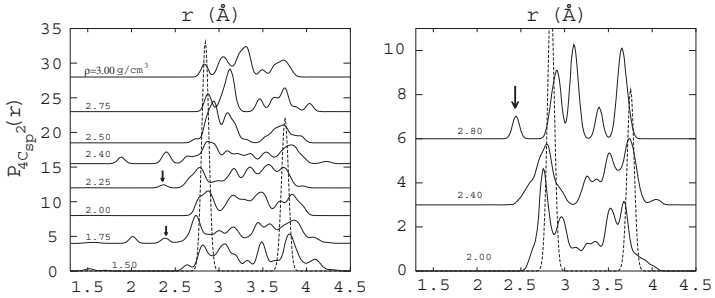

Figure 4. Mean end-to-end distance distribution function of chains of four trigonally bonded carbon atoms in hydrogen-containing amorphous carbon (left) and hydrogen-free amorphous carbon (right) at various mass densities. The corresponding distribution for graphite is superimposed as thin dashed lines.

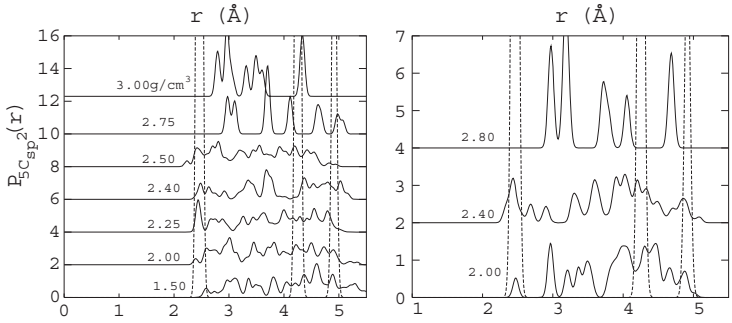

Figure 5. Mean end-to-end distance distribution function of chains of five trigonally bonded carbon atoms in hydrogen-containing amorphous carbon (left) and hydrogen-free amorphous carbon (right) at various mass densities. The corresponding distribution for graphite is superimposed as thin dashed lines.

after DFT relaxation. The distribution for the 2.0 and 2.5 g cm^{-3} systems are quite similar even for both types of relaxation. DFT relaxation causes a major increase in the population of tetrahedral bond angles for both densities.

The clustering of trigonal carbon in the generated structures has been considered. The distribution of chains of four carbon atoms all of which are trigonally bonded have been calculated. In order to determine how sp^2 carbon atoms cluster (whether as olefinic chains or rings), the end-to-end distance correlation function of such chains was evaluated. For graphite this function vanishes for all end-to-end distances except for 2.84 and 3.75 Å. The 2.84 Å feature originates from chains of four carbon atoms in six-membered rings. In figure 4 we show this distribution for the generated a-C:H (left panel) and hydrogen free-amorphous carbon (right). Superimposed on them is the distribution for graphite. The feature at 2.84 Å is observed for all densities, but a closer look at the distribution of five-membered all-sp^2-atom chains (see figure 5) shows very weak or no features at 2.4 Å (expected for true graphitic domains) for low and high densities. For the four-membered chains, no clear trend is observed for the 3.75 Å feature, indicating that there are no extended graphitic domains. The system sizes considered here do not permit us to unambiguously investigate the medium- and long-range clustering of sp^2- (trigonal-) bonded carbon atoms. Other features are seen at smaller end-to-end distances of 1.5 Å and 2–2.5 Å, respectively. These features demonstrate the presence

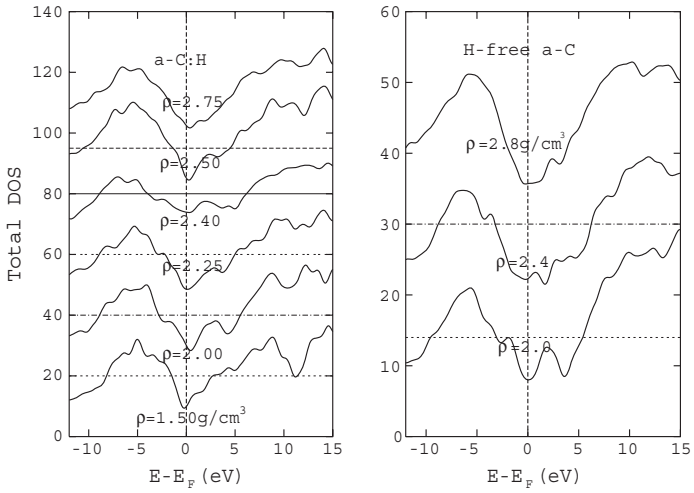

Figure 6. Total electronic density of states of 15 at.% H a-C:H and hydrogen-free amorphous carbon. The horizontal lines denote the zero DOS values for each of the densities. All the spectra have been broadened using a Gaussian with full width at half maximum of 1.0 eV.

of four- and five-fold rings of all-trigonally bonded carbon atoms, respectively. In the a-C:H systems these features show up mostly at low densities; meanwhile for a-C the 2.4 Å feature shows up at high density. The bond angle distribution for the a-C:H structures reveals that such small rings of all-sp^2 carbon atoms are highly non-planar.

Amorphous carbon and a-C:H are characterized by a disorder potential which is comparable to the stabilization energy of six-fold rings but much higher than the energy gained as a result of fusing together rings of six sp^2 carbon atoms [39, 40] to form graphitic clusters. This means that, at low temperatures, any six-fold ring that is formed would remain stable but it would require special conditions (such as annealing [7]) for the clustering of the six-fold rings to proceed. The structures generated in this work are therefore dominated by isolated rings at higher densities and olefinic or polymeric chains at low densities.

4. Electronic properties

4.1. Electronic density of states (DOS)

The electronic density of states has been evaluated for the a-C:H systems and plotted in figure 6. On the right panel of this figure the DOS of a-C is also shown for various densities. It is clear from this that the insertion of hydrogen strongly modifies the band gap region (± 2 eV around the Fermi level). For low (<2.2 g cm^{-3}) and high (>2.4 g cm^{-3}) densities the DOS in this energy range is very different from that of the intermediate graphitic density. In the latter case there is a strong increase in the DOS while for the low- and high-density systems the DOS is considerably lower. This observation is in line with the analysis of the sp^2 bond clustering that was discussed earlier: that at low and high densities fewer six-fold all-sp^2 atom chains were present in the a-C:H and that the largest proportion of these six-fold chains was recorded for intermediate densities. This trend is analogous to that observed by Frauenheim *et al* [18] on the variation of the population of four-coordinated atoms with density for high hydrogen concentrations ($\geqslant$20 at.% H). Their calculations showed that as the density was increased to 2.2 g cm^{-3} the fraction of four-coordinated atoms ('sp^3' carbon) increased but on further

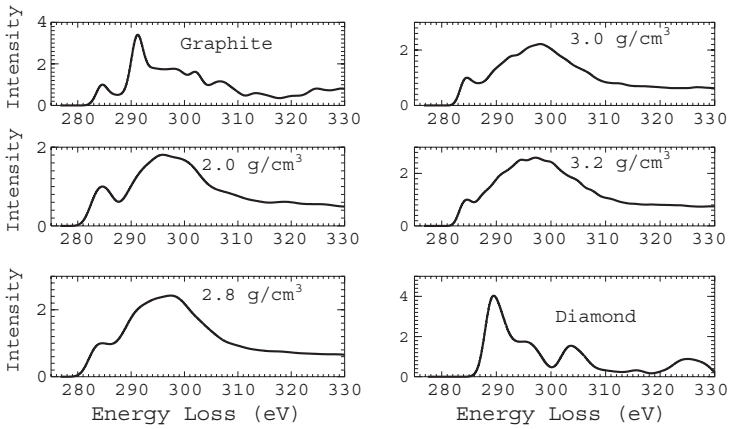

Figure 7. Carbon ELNES of graphite, diamond and hydrogen-free amorphous carbon at densities of 2.0, 2.8, 3.0 and 3.2 g cm^{-3}.

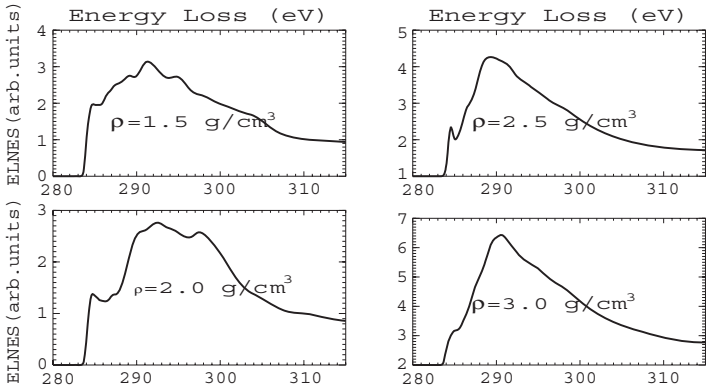

Figure 8. Carbon K-edge of 15 at.% H-containing amorphous carbon at densities of 1.5, 2.0, 2.5 and 3.0 g cm^{-3}. The core–hole effect is accounted for via the core-excited state approach.

increasing the density to 2.4 g cm^{-3} there was no major change in the 'sp^3' fraction. For densities above 2.4 g cm^{-3} this fraction grew monotonically.

4.2. Energy-loss near-edge structure (ELNES)

Considering the fact that the dipole approximation is accurate enough to enable an understanding of the ELNES spectroscopy of carbon materials [41], the interpretation of the experimental features of the XANES spectra of carbon systems based on ELNES calculations is legitimate. We shall, therefore, correlate experimentally observed XANES features of a-C:H with our ELNES calculations.

Recently we have studied the ELNES features of a-C systems [26] by using the TELNES routine of the WIEN2k code [33], and in figure 7 we have reproduced the results for different mass densities together with those of graphite and diamond. The calculated spectra for a-C:H systems are found in figure 8. The spectrum of each atom was shifted by the corresponding calculated C 1s energy and all the calculations accounted for the core–hole effect. We show the averaged spectra (averaged over all carbon atoms). From the calculated spectra of the

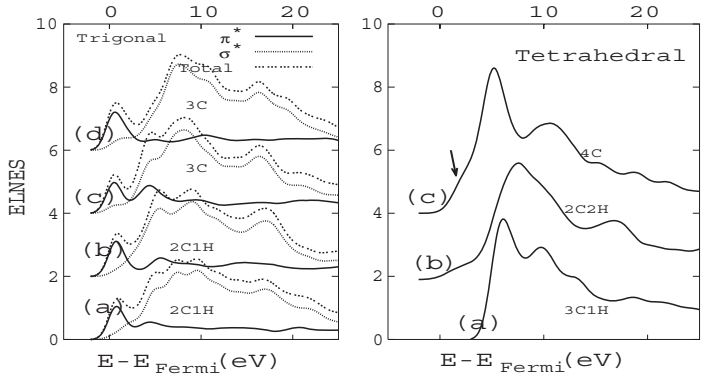

Figure 9. π^* and σ^* decomposed ELNES for selected atoms of an a-C:H at 2.5 g cm^{-3}. On the left we show the π^*, σ^* and the total ELNES of four three-coordinated atoms: two with three carbon nearest neighbours and two with two carbon and one hydrogen nearest neighbours. On the right the ELNES of some four-coordinated C atoms is shown. The arrow points to a feature resulting from stretched C–C bonds (bond length greater than 1.55 Å).

model amorphous carbon structures the sp^3 fractions deduced from them [26] were in very good agreement with those obtained by considering a microscopic structural analysis of the model a-C systems based on the π-orbital axis vector analysis [42], demonstrating that the calculated ELNES spectra correctly predict the bonding structure of the a-C structures.

For both the a-C and the a-C:H systems the usual π^* and σ^* peaks are seen at ∼285 and ∼290 eV, respectively. Intermediate between these peaks is a feature at ∼287–288 eV (it shows up as shoulders in the 2.5 and 3.0 g cm^{-3} systems) which is absent in the spectra of the a-C systems. Note that the intermediate region for the lowest density of 1.5 g cm^{-3} is quite similar to that of poly(α-methyl styrene) [23] whose spectrum is made of more than one feature within the energy range 287–290 eV. This confirms our earlier finding of section 3 that a-C:H at such low densities is polymeric.

In order to understand the origin of the 287–288 eV feature we performed orientation-resolved ELNES calculations [43] for some selected carbon atoms with well-defined local environments. Since our structures do not contain three-coordinated carbon atoms with more than one hydrogen atom as a nearest neighbour, the only possible bonding configurations are those listed in figure 9. On the left panel we show the π^*, σ^* and the total ELNES spectra of three-coordinated carbon atoms: (a) and (b) are carbon atoms with one hydrogen nearest neighbour, (c) and (d) are those with no hydrogen nearest neighbour. Spectrum (d) is that of a three-coordinated carbon atom whose nearest neighbours are also three-coordinated carbon atoms, which results in a delocalized π electron. Apart from spectrum (d), all spectra show a feature at 3–4 eV from the main π^* peak. Such a feature has been reported for the XANES spectra of a-C:H systems and is often assigned to a transition from C 1s to the C–H σ^* band [3, 6, 22]. The presence of hydrogen as a neighbour to a three-coordinated carbon atom has the tendency to enhance the localization of the π electrons of the bonds in which this atom is participating, causing the C–C bond to have some double-bond character. Graph (c), corresponding to a three-coordinated C atom with no H nearest neighbour, shows a feature at the same energy. However, this atom is participating in a double bond with another C atom. Therefore the C=C double bond can also contribute to this feature.

The next question is the character (π^* or σ^*) of this feature. A look at the π^* and σ^* components reveals that this feature has both π^* and σ^* character. It is also important to note

Table 1. Percentage of sp^3 bonding as computed by the coordination number method (method I) and the POAV analysis (method II) for DFT-relaxed a-C and 15 at.% H-containing a-C:H.

a-C:H			a-C		
Density	Method I	Method II	Density	Method I	Method II
1.50	13	15	2.00	28	37
2.00	21	24	2.40	30	32
2.25	26	30	2.80	56	59
2.50	63	68			
3.00	64	70			

that tetrahedral carbon atoms with stretched bonds ($\geqslant$1.55 Å) can also contribute in this range (see atom (c) on the right panel of figure 9). This is in line with our recent finding that the σ^* ELNES edge-onset shifts to lower energies when the C–C bond is stretched [44]. Some four-coordinated atoms, e.g. atoms (a) and (b) in the right panel of figure 9, have diamond-like ELNES spectra. This is the case of atoms connected to either hydrogen atoms or other four-coordinated carbon atoms with well-equilibrated bond lengths.

4.3. sp^3 bonding fraction

It was recently shown by us that curvature effects play a major role in the accurate determination of the sp^3 fraction of computer-generated amorphous carbon systems [31]. The sp^3 bonding fraction of such systems that is based on the coordination structure alone fails to account for the curvature-induced rehybridization that is commonly known for other curved carbon systems like fullerenes and carbon nanotubes [41]. This effect can be easily taken into account by using the π-orbital axis vector analysis (POAV) [31, 42]. The consequence of this is an increase of the sp^3 fraction by about 5–15%, especially for intermediate density carbon systems. This modified sp^3 fraction (POAV analysis) of computer-generated carbon structures has been calculated for a series of a-C and a-C:H systems. In table 1 we have shown the sp^3 percentages of a-C and a-C:H as computed using the coordination number and the POAV analysis. The local curvature of each three-coordinated carbon atom is seen to be very important for low-density a-C but seems to be weak for a-C:H. The evolution of the sp^3 fraction with density is shown in figure 10. The indicated error bars are due to (1) the statistical nature of the determination of the sp^3 fractions by the POAV analysis, which is evaluated for all three-coordinated atoms of the systems and (2) the finite system size. The latter was estimated by performing simulations for system sizes of 256 atoms and calculating the corresponding sp^3 fraction. For the a-C only the three structures corresponding to densities of 2, 2.4 and 2.8 g cm^{-3} were obtained after additional relaxation with DFT. However, our results show that the effect is small for high densities, but somewhat larger for lower densities, yet still acceptable. The results are also in good agreement with previous DFT calculations [38] and with experiments [29]. While the sp^3 fraction increases approximately linearly with the density for a-C (in accordance with ELNES measurements [29]), it seems to undergo an abrupt increase beyond a density of 2.4 g cm^{-3} for a-C:H. It should be noted that this density corresponds to the one at which sp^2 bond clustering and a maximal DOS around the Fermi level were observed. This again confirms that over the relevant density range, hydrogenated amorphous carbon may be grouped into three categories: (i) low-density polymeric amorphous carbon at densities lower than 2.2 g cm^{-3} (ii) graphitic a-C:H at densities of 2.2–2.4 g cm^{-3} and (iii) diamond-like carbon at densities above 2.4 g cm^{-3}.

Comparison with other work shows that our sp^3 fraction of 75% for a density of 3.0 g cm^{-3} a-C:H (and 15.5 at.% H) agrees very well with the 75% sp^3 obtained by Bilek *et al* [21] at a

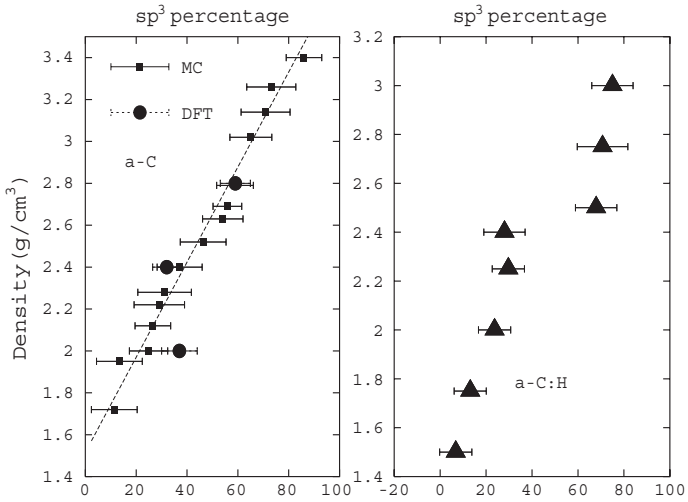

Figure 10. sp^3 fraction of a-C (left) and 15 at.% H-containing a-C (right) as a function of the mass density. The sp^3 percentages are calculated using the POAV analysis. Apart from the 2.0, 2.4 and 2.8 g cm^{-3} a-C structures, all the other a-C structures were not relaxed with DFT.

density of 2.9 g cm^{-3} and a hydrogen content of 19 at.%. At the same density their hydrogen-free amorphous carbon showed 50% sp^3, which is also in agreement with our finding. At the lower density of 2.0 g cm^{-3} and at the same hydrogen content they found 16% sp^3 (from the coordination number) while we find 24%. However, our value included a curvature effect of about 5%. The agreement for high densities is due to the fact that the POAV analysis gives similar results with coordination number for high densities [26]. The sp^3 fraction of 41% reported by Iarlori *et al* [11] for 16 at.% H in 2.6 g cm^{-3} a-C:H is quite low compared to the measured values of 60–70% [9, 29]. Our result confirms that hydrogen promotes the formation of sp^3-rich carbon systems. In a TB molecular dynamics simulation, Kopidakis *et al* [20] found that hydrogen insertion of up to 30 at.% into tetrahedral amorphous carbon (ta-C) did not modify the average coordination number of the carbon atoms.

4.4. C 1s energies

The C 1s energies of the a-C:H systems at densities of 1.5, 2.0, 2.5 and 3.0 g cm^{-3} have also been calculated within the core-excited state approximation. Figure 11 shows the distribution of the C 1s energies for the four densities. The spectra are quite similar to those of a-C systems [26]. The distribution can be fitted by a sum of two or three Gaussian functions. For a density of 2.5 g cm^{-3} four Gaussian functions were required. The fourth (but weak) peak appearing at 286.2 eV originates from the 2% five-coordinated carbon atoms that were present in that structure. For the lowest density of 1.5 g cm^{-3} two Gaussian peaks centred at 283.5 ± 0.2 and 284.4 ± 0.2 eV were required. The first peak corresponds to two-coordinated carbon atoms while the second is dominated by three-coordinated carbon atoms. As the density increased to 2.0 g cm^{-3} a third peak was required at 285.2 eV, which corresponds to four-coordinated carbon atoms. The intensity of this peak grew with further increase of density and became the dominant feature at a density of 3.0 g cm^{-3}. It should be noted that we find an energy difference of about 0.6–1.0 eV between the sp^2 and sp^3 peaks, which is in good agreement with that between graphite and diamond [37]. The calculated peak positions agree well with

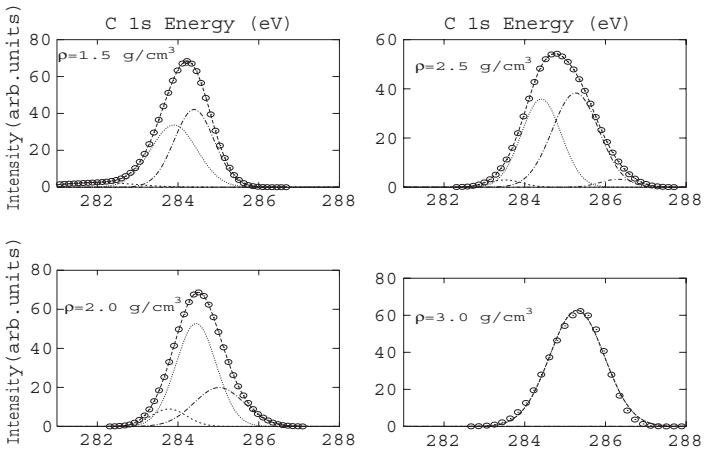

Figure 11. C 1s XPS of 15 at.% H-containing amorphous carbon at densities of 1.5, 2.0, 2.5 and 3.0 g cm^{-3}.

measurements on a-C:H [4, 5, 8]. XPS spectra of a-C:H have been resolved into three [8] or more [24, 25] features. Spectra with more than two peaks usually result from the presence of impurities (e.g. N and O). The measured full width at half maximum ranges from 1 to 1.5 eV for both pure a-C and a-C:H systems. The widths of our spectra are within this range.

5. Conclusions

We have generated amorphous carbon and hydrogenated amorphous carbon structures by a combination of classical and quantum mechanical approaches. The hydrogen content was fixed at 15 at.% while the density was varied from 1.5 to 3.0 g cm^{-3}. Partial pair correlation functions showed that the use of the short-range Brenner potential resulted in C–H second-neighbour shells having a feature at 1.8 Å. On relaxing using the density functional theory approach this feature vanished.

The calculated electronic density of states showed that hydrogen enhances the degree of disorder in amorphous carbon. Energy-loss near-edge structure calculations reveal the presence of an unoccupied electronic state intermediate between the main π^* and σ^* features. The origin of this state remains unclear. Our calculations suggest several possibilities: the presence of C–H bonds, C=C double bonds or stretched C–C σ bonds. The feature has also been shown to possess both π^* and σ^* character.

Depending on the density, three categories of a-C:H systems have been evidenced: low-density polymeric a-C:H ($\rho \leqslant 2.0$ g cm^{-3}), graphitic a-C:H (2.0 g cm^{-3} $< \rho \leqslant 2.4$ g cm^{-3}) and DLC films ($\rho > 2.4$ g cm^{-3}). We have shown that sp^2 carbon atoms have the tendency to aggregate either into isolated six-fold rings or into olefinic chains. Four- and five-fold rings of trigonal carbon atoms are also shown to be present in the low-density range.

Acknowledgments

This work was supported partly by the FWO-Vlaanderen under project G.0425.05, the IWT-Vlaanderen under contract IWT-161 and by a GOA project of the University of Antwerp entitled 'Characterization of nano-structures by means of advanced electron energy spectroscopy and filtering'.

References

[1] Donnet C and Grill A 1997 *Surf. Coat. Technol.* **94/95** 456
[2] Robertson J 2002 *Mater. Sci. Eng.* **37** 129
[3] Ray S C, Tsai H M, Chiou J W, Bose B, Jan J C, Kumar K, Pong W F, Dasgupta D and Tsai M H 2004 *J. Phys.: Condens. Matter* **16** 5713
[4] Mikami T, Nakazawa H, Kudo M and Mashita M 2005 *Thin Solid Films* **488** 87
[5] Calliari L, Filippi M, Laidani N and Anderle M 2006 *J. Electron Spectrosc. Relat. Phenom.* **150** 40
[6] Gago R, Jiménez I and Albella J M 2001 *Surf. Sci.* **482–485** 530
[7] Foulani A 2003 *J. Phys. D: Appl. Phys.* **36** 394
[8] Filik J, May P W, Pearce S R J, Wild R J and Hallam K R 2003 *Diamond Relat. Mater.* **12** 974
[9] Libassi A, Ferrari A C, Stolojan V, Tanner B K, Robertson J and Brown L M 2000 *Diamond Relat. Mater.* **9** 771
[10] Pisana S, Stephen K, O'Leary K and Zukotynski S 2005 *J. Non Cryst. Solids* **351** 736
[11] Iarlori S, Galli G and Orladina M 1994 *Phys. Rev.* B **49** 7060
[12] Godwin P D, Horsfield A P, Stoneham A M, Bull S J, Ford I J, Harker A H, Pettifor D G and Sutton A P 1996 *Phys. Rev.* B **54** 15785
[13] Jäger H U and Weiler M 1998 *Diamond Relat. Mater.* **7** 858
[14] Huang Z, Pan Z Y, Wang X Y and Du A J 2002 *Surf. Coat. Technol.* **158/159** 94
[15] Krasheninnikov A V, Nordlund K, Salonen E, Keinonen J and Wu C H 2002 *Comput. Mater. Sci.* **25** 427
[16] Alma D A and Ruzic D N 2003 *J. Nucl. Mater.* **313–316** 9182
[17] Neyts E, Bogaerts A, Gijbels R, Benedikt J and van de Sanden M C M 2004 *Diamond Relat. Mater.* **13** 1873
[18] Frauenheim T, Blaudeck P, Stephan U and Jungnickel G 1993 *Phys. Rev.* B **48** 4823
[19] Jungnickel G, Frauenheim T, Porezag D, Blaudeck P, Stephan U and Newport R J 1994 *Phys. Rev.* B **50** 6709
[20] Kopidakis G, Zang C Z, Soukoulis C M and Ho K M 1998 *Phys. Rev.* B **58** 14016
[21] Bilek M M M, McKenzie D R, McCulloch D G and Goringe C M 2000 *Phys. Rev.* B **62** 3071
[22] Kikuma J and Tonner B P 1996 *J. Electron Spectrosc. Relat. Phenom.* **82** 53
[23] Dhez O, Ade H and Urquhart S G 2003 *J. Electron Spectrosc. Relat. Phenom.* **128** 85
[24] Yan X B, Xu T, Yang S R, Liu H W and Xue J Q 2004 *J. Phys. D: Appl. Phys.* **37** 2416
[25] Meskinis S, Andrulevicius M, Kopustinskas V and Tamulevicius S 2005 *Appl. Surf. Sci.* **249** 295
[26] Titantah J T and Lamoen D 2005 *Carbon* **43** 1311
[27] Titantah J T and Lamoen D 2006 *Diamond Relat. Mater.* at press
[28] Travaly Y, Vanderbilt D and Gonze X 2000 *Phys. Rev.* B **61** 7716
[29] Ferrari A C, Libassi A, Tanner B K, Stolojan V, Yuan J, Brown L M, Rodil S E, Kleinsorge B and Robertson J 2000 *Phys. Rev.* B **62** 11089
[30] Brenner D W 1990 *Phys. Rev.* B **42** 9458
[31] Titantah J T and Lamoen D 2004 *Phys. Rev.* B **70** 75115
[32] Tersoff J 1988 *Phys. Rev. Lett.* **61** 2879
[33] Blaha P, Schwarz K, Madsen G K H, Kvasnicka D and Luitz J 2001 *WIEN2k, An Augmented Plane Wave + Local Orbitals Program for Calculating Crystal Properties* Karlheinz Schwarz, Techn. Universität Wien, Austria (ISBN 3-9501031-1-2)
[34] Perdew J P and Wang Y 1992 *Phys. Rev.* B **45** 13244
[35] Abell G C 1985 *Phys. Rev.* B **31** 6184
[36] Kohler B, Wilke S, Scheffler M, Kouba R and Ambrosch-Draxl C 1996 *Comput. Phys. Commun.* **94** 31
[37] Le Normand F, Hommet J, Szörényi T, Fuchs C and Fogarassy E 2001 *Phys. Rev.* B **64** 235416
[38] Marks N A, Cooper N C, McKenzie D R, McCulloch D G, Bath P and Russo S P 2002 *Phys. Rev.* B **65** 75411
[39] Robertson J 1995 *Diamond Relat. Mater.* **4** 297
[40] Robertson J 1997 *Diamond Relat. Mater.* **6** 212
[41] Titantah J T, Jorissen K and Lamoen D 2004 *Phys. Rev.* B **69** 125406
[42] Haddon R C and Scott L T 1986 *Pure. Appl. Chem.* **58** 137
[43] Nelhiebel M, Louf P H, Schattschneider, Blaha P, Schwarz K and Jouffrey B 1999 *Phys. Rev.* B **59** 12807
[44] Titantah J T and Lamoen D 2005 *Phys. Rev.* B **72** 193104